Predictive control for a single-blow cold upsetting using surrogate modeling for a digital twin

David Uribe[1] · Cyrille Baudouin[1] · Camille Durand[1] · Régis Bigot[1]

Abstract
In the realm of forging processes, the challenge of real-time process control amid inherent variabilities is prominent. To tackle this challenge, this article introduces a Proper Orthogonal Decomposition (POD)-based surrogate model for a one-blow cold upsetting process in copper billets. This model effectively addresses the issue by accurately forecasting energy setpoints, billet geometry changes, and deformation fields following a single forging operation. It utilizes Bézier curves to parametrically capture billet geometries and employs POD for concise deformation field representation. With a substantial database of 36,000 entries from 60 predictive numerical simulations using FORGE® software, the surrogate model is trained using a multilayer perceptron artificial neural network (MLP ANN) featuring 300 neurons across 3 hidden layers using the Keras API within the TensorFlow framework in Python. Model validation against experimental and numerical data underscores its precision in predicting energy setpoints, geometry changes, and deformation fields. This advancement holds the potential for enhancing real-time process control and optimization, facilitating the development of a digital twin for the process.

Keywords Surrogate model · Forging processes · POD · Numerical simulation · Data-driven model · Bézier Curves

Introduction

In the domain of forging processes, achieving the desired product involves fulfilling multiple requirements, encompassing both geometric and mechanical criteria. To attain this, one of the crucial tasks involves defining optimal process control parameters during the conception stage. This is usually accomplished by employing numerical, experimental, and optimization methods [1]. However, it's essential to note that these parameter definitions are often based on nominal conditions, neglecting the variabilities inherent in every process [2], and creating product specification deviations [3–5].

✉ David Uribe
david_santiago.uribe_espitia@ensam.eu

Cyrille Baudouin
cyrille.baudouin@ensam.eu

Camille Durand
camille.durand@ensam.eu

Régis Bigot
regis.bigot@ensam.eu

[1] HESAM Université, Arts et Métiers Institute of Technology, Université de Lorraine, LCFC, F-57070 Metz, France

Various control predictive models can be employed to tackle this challenge, ranging from analytical approaches like the slab method [6], which offers reactivity but lower accuracy, to numerical simulations[7], which provide higher accuracy but come with increased computation time.

The trade-off becomes apparent for real-time control of forging processes: the analytical models are fast but lack precision, while the numerical simulations are accurate but time-consuming. As a solution, surrogate models emerge as a crucial element for real-time predictions, striking a balance between reactivity and accuracy. Surrogate models, which are statistical representations of complex systems or processes, are data-driven models constructed using design of experiments (DoE) and interpolation methods[8]. These models provide an efficient alternative by creating a simplified representation that captures the crucial relationships between input variables and output responses [9].

In the field of metal forming, researchers [10, 11] have explored the utility of these surrogate models for tool design. Additionally, various applications in hot rolling processes have been conducted, such as rolling force prediction [12–14] and, strip crown prediction [15–17]. Within stretching processes, they have been combined with analytical models to predict plastic strain [18]. Similarly,

they have been coupled with semi-analytical models of the press to forecast the efficiency of the forging blows in upsetting operations [19]. Moreover, in extrusion, [20, 21] investigated the influence of process variables on forming behavior using surrogate models.

In certain applications, the scope of surrogate models extends beyond scalar predictions, necessitating the description of complete fields, such as deformation fields. To construct such models, Proper Orthogonal Decomposition (POD) is widely employed to reduce their dimensionality and facilitate their description, leading to what is known as POD-based surrogate models [22–24]. These models leverage the dimensionality reduction capabilities of POD to efficiently represent complex fields and improve the overall efficiency and accuracy of the surrogate modeling process.

While POD-based surrogate models have been studied in sheet metal forming processes, focusing on process force–displacement curves [25], displacement vectors [26], and springback compensation [27, 28] POD frameworks, their potential in bulk metal forming processes remains relatively unexplored.

On the other hand, while working with bulk forming processes, a common challenge arises due to the presence of complex geometries that pose significant difficulty in direct parametrization for surrogate modeling. These intricate shapes often require a reduced parametric description before they can be efficiently represented using a surrogate model. One promising approach to address this issue is through the use of Bézier curves for parametric representation of the geometries and curves[29, 30]. Bézier curves offer a flexible and efficient way to describe complex shapes using control points and curve segments [31, 32].

This present paper proposes a POD-based surrogate model to approximate the energy setpoint (piloting variable), deformation field, and geometry of a copper billet during a one-blow cold upsetting process in a screw press. To achieve a reduced representation of the deformation fields, the widely employed POD method has been utilized. Additionally, considering the axial symmetry of the billet, the geometry is represented as a profile, known as the "bulging profile," effectively parametrized using Bézier curves. An artificial neural network control predictive model has been developed to integrate different process variables with parametrized fields and geometries, forming the foundation for the development of a digital twin for the forging operation.

Materials

Experimental Setup

The metal-forming machine used for the study is the screw press LASCO SPR400® (see Fig. 1a), installed in the VULCAIN platform of the Laboratory of Design, Manufacturing, and Control (LCFC) at Metz, France. This press can deliver a maximum forging energy of 28.9 kJ for a maximum ram speed of 680 mm/s. It is part of the energy-controlled machines. For this press, the energy setpoint is introduced as an integer value from 1 to 100, being a percentage of the maximum energy. Adjusting this energy setpoint turns into controlling the ram speed before it impacts the billet.

The study focuses on the cold one-blow upsetting process of cylindrical billets made of pure copper. These billets encompass a range of initial diameters spanning from 18 to 32 mm, with upsetting ratios (height/diameter) ranging

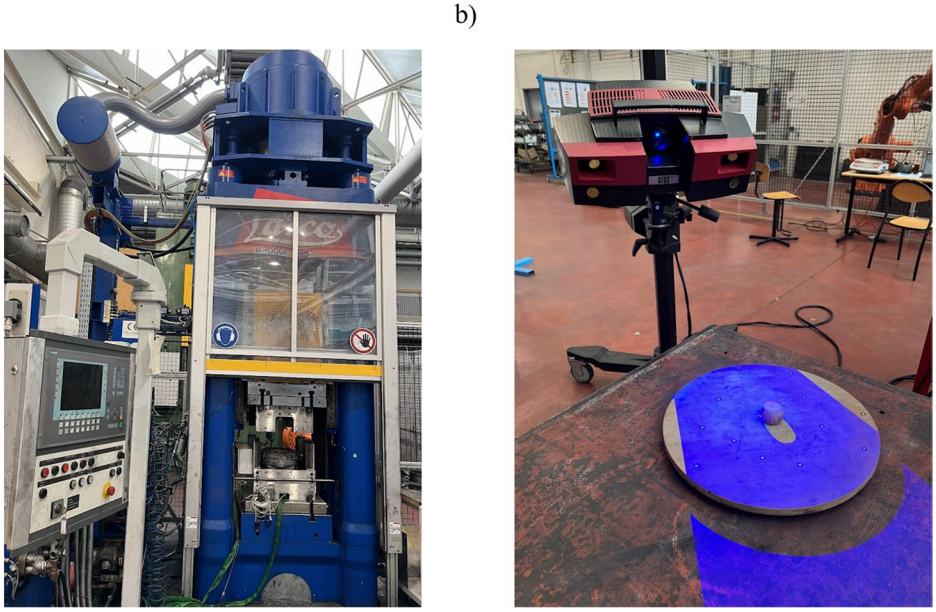

Fig. 1 Experimental setup: **a** Energy-controlled screw press. **b** Optical 3D scanner

between 1.5 and 2.5. A graphite-based aerosol lubricant has been used. For this operation, the tooling is mounted on the press and it is equipped with flat surface dies positioned both at the top and bottom. During the forming operation, the billet, characterized by its initial diameter (D_i) and initial height (H_i), undergoes forging along its axis of revolution and is transformed into a forged part with a final height, and its original cylindrical shape is altered due to friction conditions, leading to the formation of a bulging profile (see Fig. 2).

A high-resolution 3D optical scanner GOM ATOS II Triple Scan® (see Fig. 1b) was utilized to extract the final geometry of the billets, with specific attention to the bulging profile. To enhance the accuracy of the measurements, the billets were coated with titanium oxide powder to reduce light reflection and improve surface contrast. Each billet's resulting 3D file (.stl) was then processed using GOM Inspect® Software to extract the final height and bulging profile as scattered points.

Numerical Setup

Numerical simulations have been implemented using the commercial software FORGE® by Transvalor. The assumption of axial symmetry is made, enabling a denoted 2D simulation and resulting in reduced computational costs (See Fig. 3).

The reduced Hansel-Spittel constitutive equation has been employed to represent the billet's rheology, where the flow stress σ_s is denoted as:

$$\sigma_s = A \cdot e^{m1 \cdot T} \cdot \varepsilon^{m2} \cdot \dot{\varepsilon}^{m3} \cdot e^{m4/\varepsilon} \quad (1)$$

where ε and $\dot{\varepsilon}$ are strain and strain rate respectively; T is the temperature; $A, m1, m2, m3, m4$ are material constants, with specific values of 411.19, -0.00121, 0.13, 0.01472, and 0.002 respectively, as the numerical model was rigorously validated against experimental data to ensure accuracy. Material physical properties are listed in Table 1.

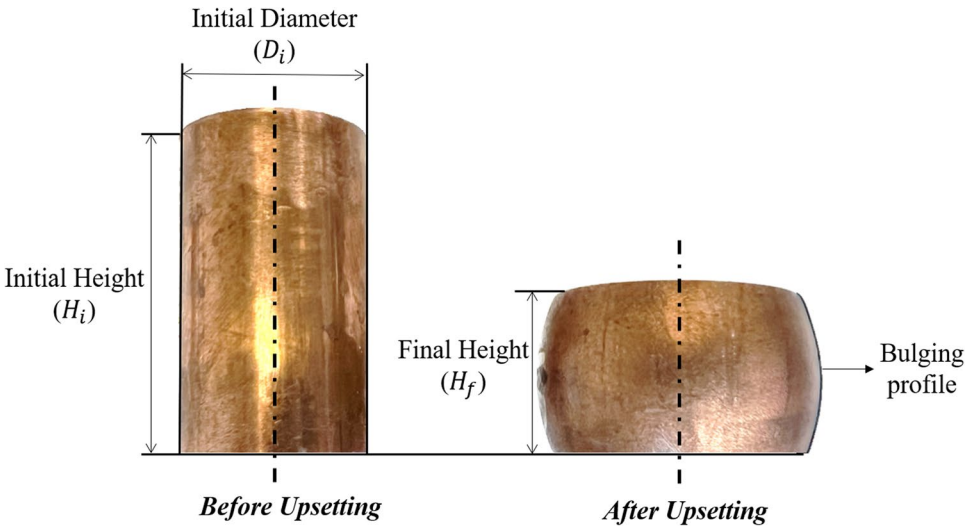

Fig. 2 One-blow cold upsetting of a copper billet

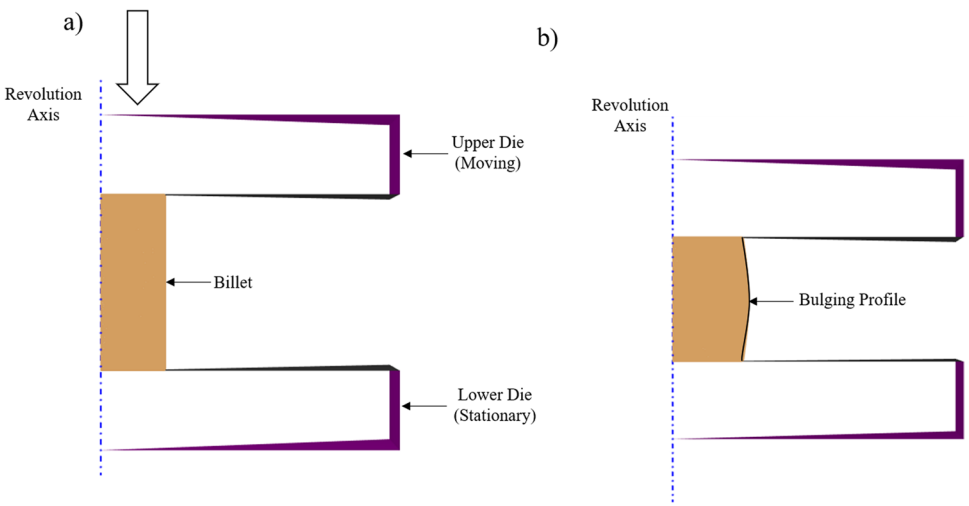

Fig. 3 One-blow cold upsetting numerical setup: **a** Before Upsetting, **b** After upsetting

Furthermore, thermal exchanges have been assumed at $2000W/m^2K$ between the billet and the tools, and at $10W/m^2K$ between the air and the billet. Friction conditions follow a Coulomb limited Tresca Model:

$$\tau = \min\left(\mu \cdot \sigma_n; \overline{m} \cdot \frac{\sigma_s}{\sqrt{3}}\right) \tag{2}$$

where σ_n is the contact pressure; μ and $\overline{m}$ the friction coefficients, equal to 0.1 and 0.2, respectively.

The room temperature is 20 °C, which is also the initial temperature of the billet and the tools.

The meshing of the billet consists of tetrahedrons with an average surface mesh size of 0.2 mm. Initial billet diameters vary within the range of 15 mm to 35 mm, while the initial upsetting ratios (Height/Diameter) fall within the span of 1.5 to 2.5. The press is modeled with two rigid dies, and its behavior adheres to that of the experimental setup. On average, the computational time amounts to 15 min for one case $(D_i, H_i, Energy_i)$.

This numerical model forms the basis for the training database used in this study.

Methods

Description of the billet's geometry using a parametric Bézier curve

To accurately represent the bulging profile of the billet after upsetting, a parametric approach using Bézier curves is used. These curves are a widely used mathematical technique for creating smooth and continuous curves based on control points [33, 34]. They are denoted as the path defined by the function B_n, referred to as the Bézier polygon or the B-polygone, as outlined below [35]:

$$B_n(P_0, P_1, \ldots, P_n; t) = \sum_{i=0}^{n} b_i^n(t) P_i \quad 0 \le t \le 1 \tag{3}$$

where the points $P_0, P_1, \ldots, P_n$ are called the control points (CPs) of the Bézier's curve placed in 2D/3D coordinates, n the degree of the B-polygon, and $b_i^n(t)$ are known as the Bernstein basis polynomials of degree n. The notable advantage of employing these types of curves is rooted in the concept of CPs, which constitute a set of coordinates facilitating the parametric representation of multiple curves. The determination of the appropriate quantity of CPs to utilize in a specific scenario depends on the degree of the curve being represented

Table 1 Physical properties of billet at 20°C

Material	Young's modulus (MPa)	Poisson's ratio	Density (kg/m3)	Thermal conductivity (W/m–K)	Specific heat (J/kg-K)
Pure Copper	110,000	0.3	8100	401	435

In cases of experimental geometries obtained through optical scanning, complete axisymmetric conditions cannot be guaranteed. To represent a single profile of the billet's bulging section, 36 profiles are extracted at 10-degree intervals around the axis of revolution. Subsequently, an average discretized section is derived in the 2D plane, accompanied by an associated uncertainty value.

In numerical 2D simulations, perfect axial symmetry is assumed, simplifying the representation of geometries in the plane using a set of 2D coordinates. The number of these coordinates varies depending on the billet's dimensions and the simulation mesh size.

Once both types of geometries, numerical and experimental, are represented in the plane, a discretization process is applied using a regular horizontal grid. This step ensures consistency and enables comparisons among different billets. The process involves conducting linear interpolation along the axis of revolution to standardize the number of 2D coordinates used to represent any billet (refer to Fig. 4a).

For a precise depiction of the different billets, encompassing both experimental and numerical cases, around 30 to 50 points are needed to ensure an accurate representation of the overall profile of the geometry and the bulging profile (see Fig. 4b–c).

To find the coordinates of the Bézier CPs, an optimization algorithm is implemented in Python. The aim is to find the optimal coordinates of different numbers of CPs which minimizes the mean squared error (MSE) between the reconstructed and the original points. The results indicate that the performance does not exhibit a significant decrease beyond the utilization of 5 control points, where the root mean square error (RMSE) is 0.026 mm, and any enhancements observed are below 0.01 mm. Therefore, 5 control points have been selected to represent the different bulging profiles, using a total of 10 data points (2 coordinates for each control point), as illustrated in Fig. 5a.

The upper and lower symmetry, as well as the axial symmetry, are assumed. So, a new variable convention is adopted to minimize the number of parameters required to describe the bulging profile. These parameters, named $a, b, c, r_{min} and h$ can be observed in Fig. 5b.

Description of the deformation fields using a parameterized vector system through Proper Orthogonal Decomposition (POD)

Deformation fields are derived from numerical simulations. They are represented by triangular elements with node

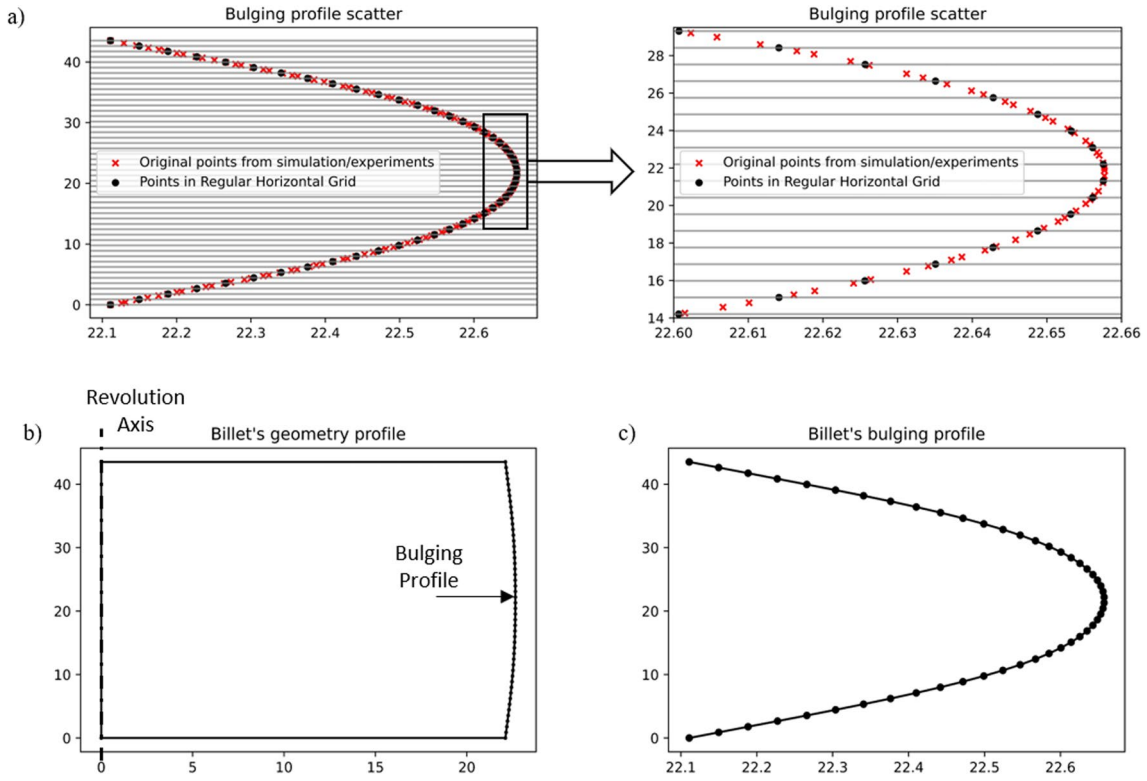

Fig. 4 2D Scattered points: **a** Discretization process in numerical/experimental profiles, **b** Overall billet's geometry after discretization (**c**) Billet's bulging profile after discretization

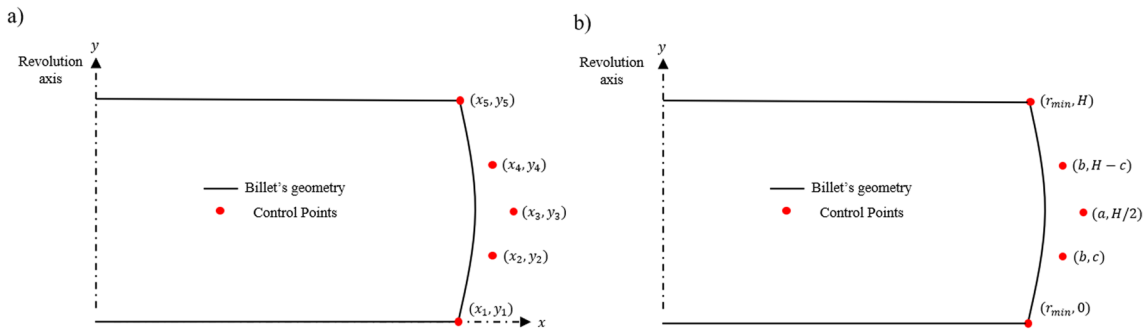

Fig. 5 Parametric representation of the bulging profiles: **a** CPs coordinates, **b** Reduced parameter representation

coordinates and corresponding unitary deformations at the barycenter of each element in the 2D plane. The large number of elements (which can differ from one simulation to another) doesn't permit real-time applications.

To be able to represent deformation fields in real time and to integrate them into a further model, it is necessary to establish a reduced parametrized representation. The Proper Orthogonal Decomposition (POD) technique is used for this purpose. This technique allows the characterization of the fields through a parameterized vector system, which captures their dominant features or patterns. By selecting the most influential vectors (also called modes), the quantity of data needed to represent accurately the deformation fields is reduced.

The number of elements in the simulation's mesh can vary depending on the size of the billet. To ensure a uniform representation of the fields before implementing the POD, a discretization process is employed, converting each deformation field into a matrix format of 100×100. This matrix discretization involves incorporating horizontal grids along the billet's height and curved vertical grids along the billet's radius, as illustrated in Fig. 6. The selection of a 100×100

matrix size was determined through gradient analysis of the subsequent field. To determine the deformation values for each point of the matrix, an interpolation method utilizing specific Delaunay triangulation was employed [36]. This approach enables the accurate estimation of deformation values within the standard discretized matrix for a comprehensive representation of the billet's deformation field.

Once the discretization process is defined, the POD is applied to a database constructed using numerical simulations. The objective is to represent any deformation field using the same vector modes while allowing for changes only in the vector coefficients. To achieve this, the database used for the POD must encompass a wide range of deformation behaviors observed during the upsetting operation. To fulfill this, a reduced design of experiments consisting of 50 simulations was devised using a Latin Hypercube Sampling, covering the same operational range of the surrogate model. This range encompassed billets with initial diameters ranging from 15 to 50 mm and slenderness ratios (H_i/D_i) between 1.5 and 2.5.

From each simulation, an average of 740 snapshots was extracted, resulting in a total of 37,000 snapshots representing various billet configurations and deformation states. For applying the POD technique, each snapshot is discretized as presented before, then vectorized into a 10,000-size vector (from 100×100 matrix), and finally stored in a single database matrix $37{,}000 \times 10{,}000$, which is centered and standardized to improve the POD results.

The results of the POD analysis revealed that the first mode exhibited a significantly higher singular value compared to the rest, capturing over 75.5% of the total energy in the dataset. As additional modes were considered, the cumulative sum of the first two, three, and four modes increased to 79.8%, 81.7%, and 82.9%, respectively. This represented an improvement of 4.8%, 1.9%, and 1.2% for each additional mode (see Fig. 7 and Table 2).

To evaluate the accuracy of the reconstructed deformation fields, we computed the Mean Squared Error (MSE), Mean Absolute Error (MAE), and Mean Absolute Percentage Error (MAPE) between the generated 100×100 matrices fields from simulations and those generated with different numbers of modes (see Table 2).

Observing that the first three modes captured more than 80% of the cumulative energy in the dataset, and additional modes did not significantly reduce errors, the decision was made to utilize only these three modes to represent deformation fields within our operational range. While the incorporation of supplementary modes could yield enhanced precision, factors such as computation time, the requisite variables for representation, and storage considerations had to be considered.

Surrogate model's architecture and database creation

The primary objective of the surrogate is to predict three key aspects: the energy setpoint, the geometry, and the deformation field for a forged billet based on its initial geometry (H_i, D_i) and the desired final height (H_f).

The parametric representation of the bulging profiles and the Proper Orthogonal Decomposition (POD) framework for the deformation fields allows for dealing exclusively with scalar variables in both the inputs and outputs, as illustrated in Fig. 8.

As the surrogate model relies on data-driven techniques, the establishment of a reliable database becomes imperative for its training process. The same simulations that were employed for constructing the POD framework were utilized to generate the surrogate database. This database was designed using a Design of Experiments (DoE), involving the deliberate manipulation of factors, namely the D_i, the slenderness ratio (expressed as $SR = H_i/D_i$) and the ES.

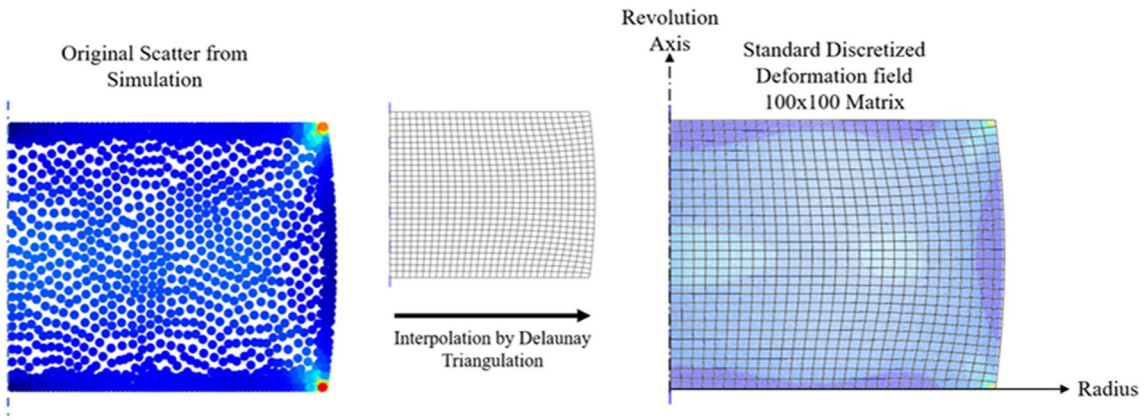

Fig. 6 Standard discretization using interpolation by Delaunay triangulation for representing the deformation fields in 100×100 matrix

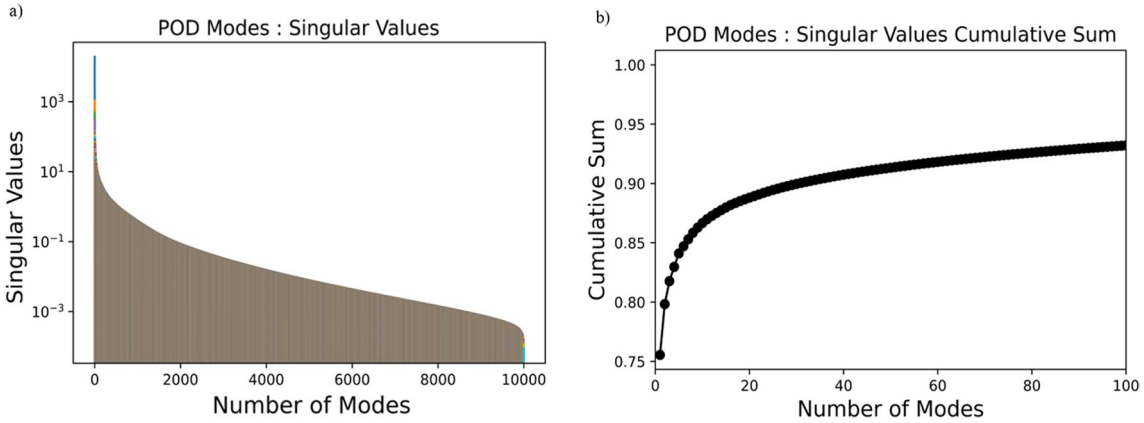

Fig. 7 POD results: **a** Singular values. **b** Singular values cumulative sum

Table 2 Choice of the number of modes: errors between the discretized fields and the fields generated with the POD framework

Number of modes	*Cumulative Energy*	Δ*Cumulative Energy*	MAPE [%]	MSE	MAE
1	75.55%	75.55%	0.335	0.00471	0.0210
2	79.83%	4.28%	0.332	0.00152	0.0209
3	81.77%	1.94%	0.167	0.00086	0.0121
4	82.97%	1.20%	0.159	0.00061	0.0113
5	84.10%	1.13%	0.121	0.00039	0.0078
100	93.21%	9.11%	0.016	0.00001	0.0015

Incorporating the *SR* and *ES* instead of the H_i and H_f as outlined in the surrogate model's input–output architecture carries noteworthy implications. First, the H_i must adhere to the experimental buckling constraint dictated by the *SR*, a prerequisite aimed at averting undesirable buckling occurrences. Secondly, the substitution of the H_f with the *ES* arises from a practical consideration. The H_f is a parameter not easily manipulable in numerical simulations, which can limit its usefulness as a factor in the design of experiments. In contrast, the *ES* is intentionally selected owing to its inherent correlation with the H_f.

In essence, this strategic selection of input parameters brings enhanced practicality and alignment with real-world constraints to the database creation process, bolstering the overall effectiveness and reliability of the subsequent surrogate model's training.

A reduced DoE Latin Hypercube Sampling of 50 combinations is performed for the following variation ranges:

- $D_i = [15 - 50]\text{mm}$
- $SR = H_i/D_i = [1.5 - 2]$
- $ES = [0 - 60]\%or[0 - 17.34]kJ$

Each simulation is performed and the results are processed to have the inputs and outputs scalar magnitudes as presented in Fig. 8. From each simulation, an average of 740 snapshots (computation increments) were taken, for a total of 37,000 combinations of the dataset.

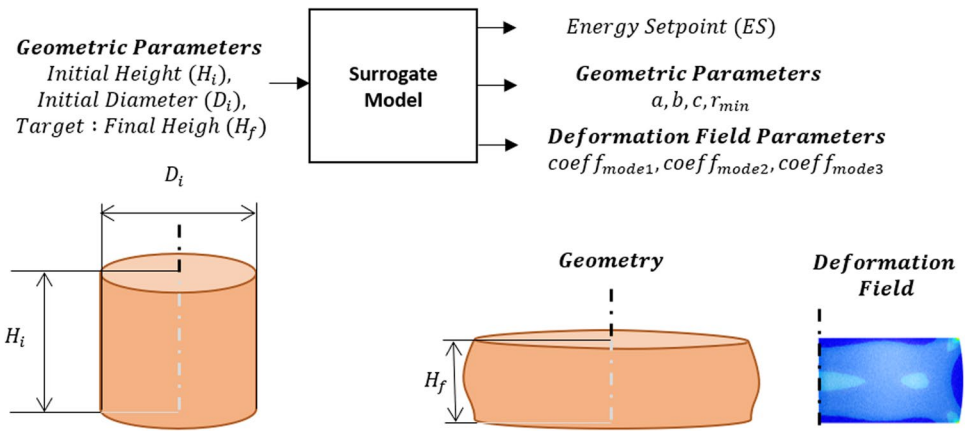

Fig. 8 Surrogate model's inputs/outputs (I/O) architecture

Surrogate model's training, testing, and validation

The utilization of the surrogate model aims to establish a correlation between input and output variables. Leveraging a limited dataset derived from a finite number of numerical simulations, the primary objective involves employing interpolation techniques to extend insights across its domain. This objective is pursued through the implementation of a multilayer perceptron artificial neural network. The standard protocols for training, testing, and validation commonly employed in such contexts will be adhered to.

Initially, the input variables in the database were normalized to bring them within a similar range by using their minimum and maximum values. Next, the database was divided into training and testing datasets in an 80–20 ratio. The selected architecture for the network includes three hidden layers with 92, 184, and 24 neurons, respectively, using the Rectified Linear Unit (ReLU) activation function. Additionally, a linear activation function was opted for the output layer. The loss function is the MSE. During the training and testing processes, the model demonstrated an adjusted coefficient of determination (R2) exceeding 0.99 and MAPE below 1%. For the energy setpoint prediction, being the key piloting variable, the MAE was below 0.1 kJ and the Root Mean Squared Error (RMSE) was below 0.15 kJ. Notably, both values were well below the minimum controllable energy of 0.289 kJ, equivalent to 1% of the maximum forging energy.

The validation process consisted of a single campaign that included both experimental and numerical tests conducted using identical process parameters. The experimental results were employed to validate the accuracy of geometric predictions, such as the final height and bulging profile. Meanwhile, the numerical results were employed to validate not only the geometry predictions but also the subsequent deformation field, which is challenging to measure directly in a real billet.

In the validation campaign, specific billets were carefully selected, ensuring they were within the training limits of the model. These chosen billets were verified to be different from the ones used in the training and testing stages. They were measured before upsetting with a caliper with a tolerance of 0.05 mm. A single blow was performed for each billet, followed by a corresponding simulation using the same process parameters to analyze and evaluate the results.

Results

Four billets were chosen for the validation. For each billet, different upsetting energy was imposed as it is the piloting variable of the process. The billets' final geometry was extracted using the 3D optical scanner. The experimental final heights served as input parameters for the surrogate model, which enabled the prediction of the energy setpoints, geometric parameters, and deformation fields.

The prediction of the energy setpoint has errors below 0.2 kJ for all the billets (see Table 3), which corresponds to less than the minimum controllable energy of the machine, which is 0.289 kJ, assuring the piloting of the process at ±1% of the machine's capabilities.

To verify the accuracy of the geometry prediction, the average profiles of each billet scan are compared against those reconstructed using the predicted Bézier parameters, and those obtained using new numerical simulations performed with the same process parameters for obtaining the same final height. As shown in Figs. 9 and 10, the prediction of the resulting bulging profile is accurate for all the cases, with a maximum gap below 0.1 mm between the surrogate and the experimental profiles, and under 0.03 mm between the surrogate and the numerical profiles. For the four experimental scenarios, the average Root RMSE and MAPE between the surrogate and experimental profiles are 0.08 mm and 0.39%, respectively. Correspondingly, between the numerical simulations and the experimental profiles, the average values stand at 0.06 mm for RMSE and 0.26% for MAPE.

The predicted deformation field by the surrogate model is compared to the one obtained using the numerical simulation for all the cases. The errors obtained are below 0.038 for RMSE and 1.17% for MAPE. Additionally, the gap between the mean deformation of the billets (predicted and numerical) in each case remains under 0.0035, while the maximum error between two deformation values at the same billet location remains below 0.017. The generated fields and the difference between them (simulated – predicted) are presented for case II in Fig. 11.

Table 3 Billet index – validation campaign

Case	Initial diameter (D_i)	Initial height (H_i)		Energy setpoint: experimental	*Experimental:* final height (H_f)	Energy setpoint: prediction	
I	24 mm	33.20 mm	4%	1.15 kJ	25.80 mm	3.79%	1.09 kJ
II		37.75 mm	9%	2.60 kJ	24.40 mm	8.61%	2.48 kJ
III	32 mm	44.30 mm	14%	4.04 kJ	32.15 mm	13.42%	3.88 kJ
IV		56.85 mm	30%	8.67 kJ	33.00 mm	29.37%	8.49 kJ

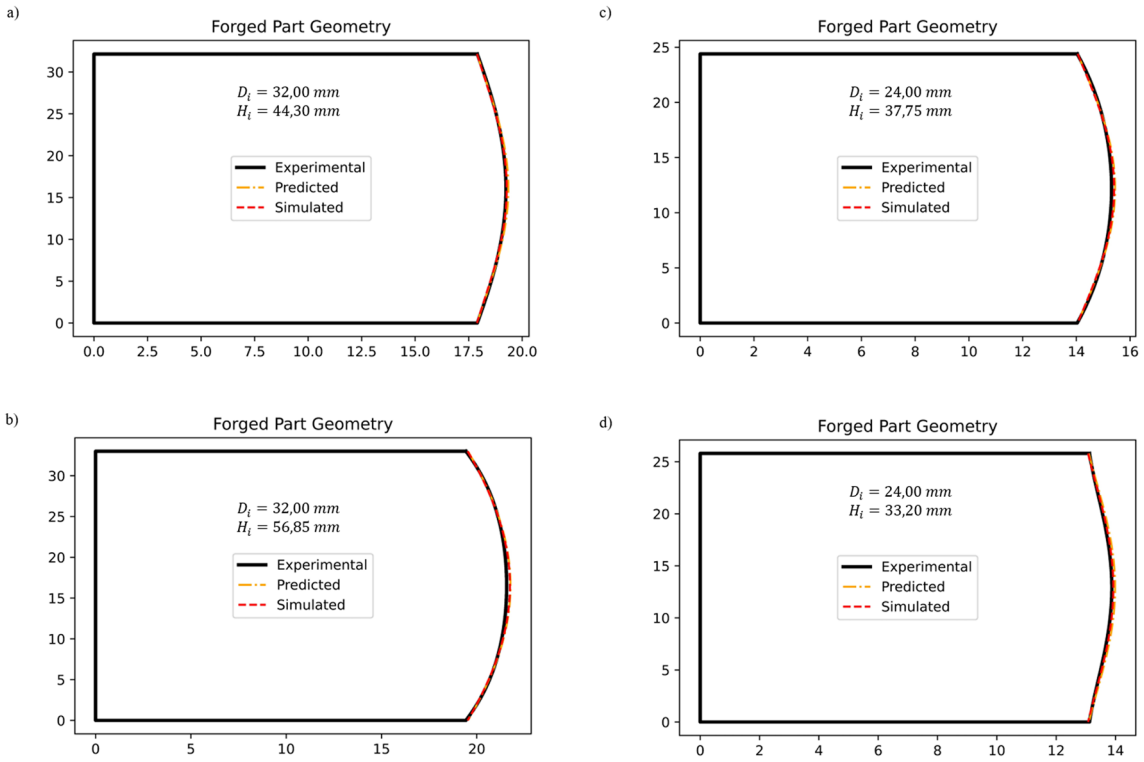

Fig. 9 Reconstructed geometry of the billets: **a** Case I, **b** Case II, **c** Case III, **d** Case IV (See Table 3)

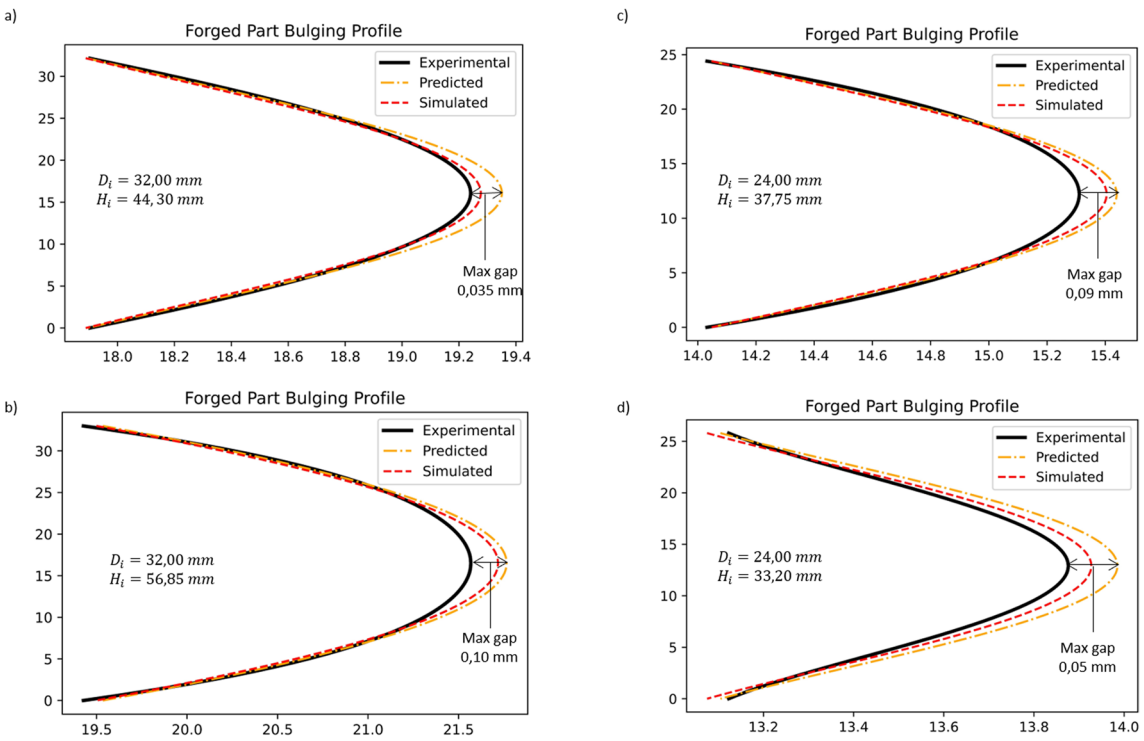

Fig. 10 Reconstructed bulging profiles: **a** Case I, **b** Case II, **c** Case III, **d** Case IV ((See Table 3)

Discussion

- By employing Bézier's control points to represent various bulging profiles, a reduced parametrization was achieved, ensuring an accurate representation of different upsetting geometries with only 5 parameters (assuming symmetry in the upper and lower sections of the billet). However, to strike a balance between parameterization reduction and surface representativity, it is crucial to implement proper optimization algorithms to determine the appropriate number of control points. Since additional parameters to predict can make difficult the training of the model.

  Careful consideration must be given to the profile discretization process, and the symmetric hypothesis made, as they could affect the profile reconstruction.
- Furthermore, while utilizing the POD framework for representing deformation fields, several important considerations come into play:

  – The interpolation used for discretization and standardization of the fields introduces errors that can vary in significance depending on the chosen interpolation technique. Consequently, careful selection of the most appropriate interpolation method is vital to minimize these errors. In our case, a method utilizing specific Delaunay triangulation was employed.
  – Careful consideration must be given to selecting the number of modes, considering their sensitivity to variations in the deformation field. Setting an overly sensitive mode could hinder the model's training without yielding substantial improvements in accuracy.

While the results obtained from the POD framework are satisfactory, other dimensionality reduction techniques could be explored, such as convolutional neural networks (CNNs), as demonstrated in [37] for geometry description in preforms and stamped parts.

POD offers clear advantages over CNNs in specific scenarios, including interpretability, dimensionality reduction, reduced training time, low data requirements, suitability for linear systems, and robustness to noisy data. However, CNNs are better suited for tasks involving complex visual data and non-linear patterns. Therefore, when dealing with more intricate deformation fields or geometries in other forging operations, it is crucial to consider evaluating the use of CNNs as well.

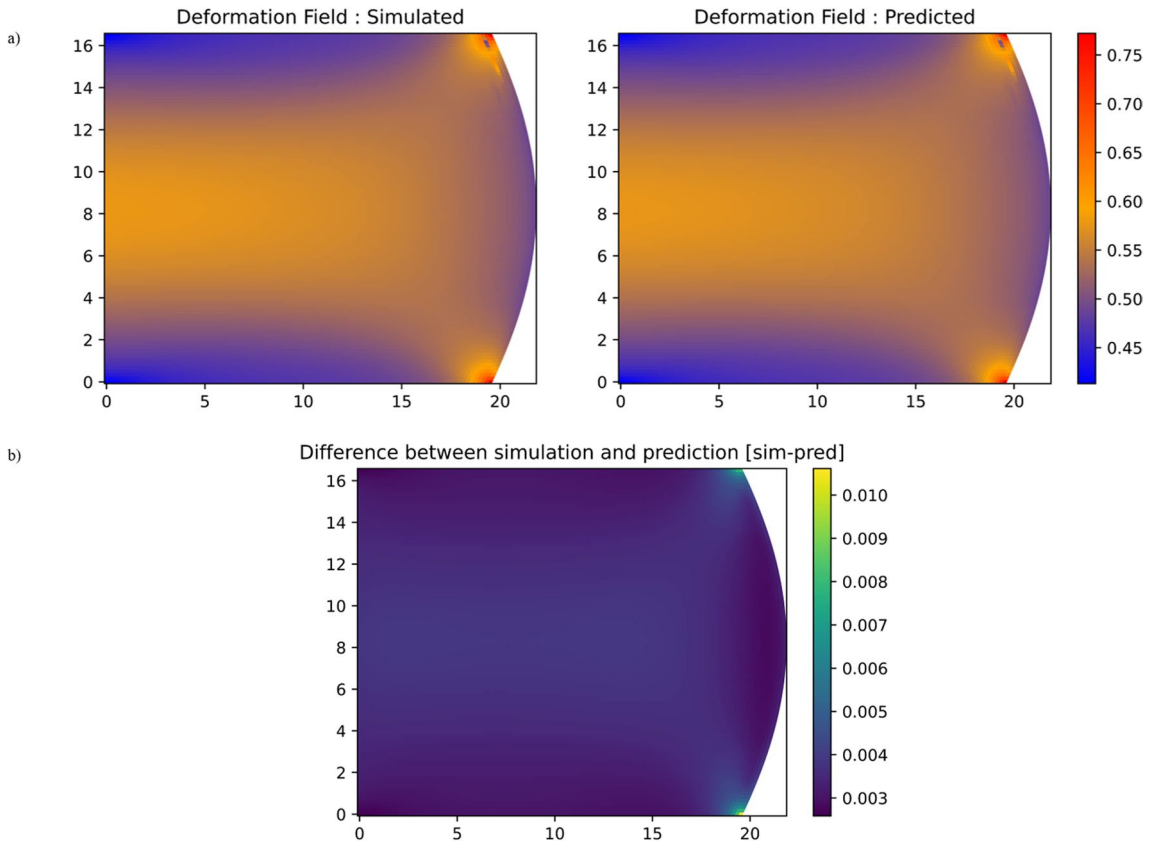

Fig. 11 Results of the deformation field for case II. **a** deformation field simulated and predicted (**b**) difference (simulated-predicted)

In comparison to the conventional analytical slab method, which neglects the bulging profile and assumes a cylindrical billet throughout the operation, the proposed model significantly improves geometry prediction. Additionally, compared to the classical numerical simulations, the proposed model exhibits remarkable responsiveness, with computation times approximately 900 times faster (compared to 'fast' 2D simulations), completing calculations in less than 1 s, while maintaining high-quality results.

The accurate geometry, energy setpoint, and deformation state predictions provided by this model offer the potential to develop a multiple-blow operation model, where metal hardening and changes in geometry play important roles. However, the model consistently underestimates the amount of energy needed for each operation. This discrepancy may be explained by not taking into account the energy losses during the forging operation, a factor that increases with subsequent blows and significantly influences energy consumption throughout the process [38]. Further investigation into energy losses and their inclusion in the model could improve the energy prediction accuracy.

Additional research efforts should also be directed toward other forging operations such as closed-die forging, where the material flow is controlled, or towards hot forging operations, where the time-dependent thermal behavior of the parts plays a crucial role.

Conclusion

This study presents the development of a POD-based surrogate model for controlling a copper cold upsetting operation. The model successfully predicted the energy setpoint, ensuring precise machine piloting. Additionally, it accurately forecasted the subsequent bulging profile using Bézier curves for parametric representation, and the deformation field was efficiently described, approximated, and reconstructed using a POD framework.

In summary, the methodology implemented in this study facilitated a systematic simplification of various challenges. Initially, it translated complex geometric issues into scalar problems via the utilization of Bézier curves. Subsequently, a similar simplification was applied to field descriptions using the POD framework. Ultimately, the surrogate model's application allowed for responsive predictions of these parametric variables in conjunction with other process variables, resulting in a robust correlation between experimental and predicted outcomes. In this context, this model serves as a foundational element for the deployment of a digital twin.

Further investigations are warranted to incorporate the blow's efficiency and the thermal state of the part, which are expected to enhance the model's overall performance and accuracy.

Acknowledgements We would like to sincerely thank the Technical Center for Mechanical Industry (CETIM) for their financial support in this research project. Specifically, we would like to thank Pierre KRUMPIPE, Stéphane MAGRON, and Valérie SULIS for their project follow-up and advice. We would also like to thank Francisco CHINESTA, a university professor and researcher at the Laboratory for Processes and Engineering in Mechanics and Materials (PIMM), for his contribution to this project through his expertise in dimensional reduction and surrogate models. Finally, we would like to thank Sébastien BURGUN and Alexandre FENDLER for their technical support during the various tests conducted.

Author's contributions DU: Investigation, Data curation, Software, Writing-original draft, Writing-review & editing; CB: Methodology, Formal Analysis, Writing- review & editing; CD: Conceptualization, Validation, Writing-review & editing; RB: Resources, Supervision, Writing–review & editing, Funding acquisition.

Funding This study was funded by the Technical Center for Mechanical Industry (CETIM) and the Carnot Institut ARTS (Research Actions for Technology and Society).

Declarations

Competing interests The authors have no competing interests to declare that are relevant to the content of this article.

References

1. Ji H, Wu W, Song C, Li J, Pei W, Huang X (2022) Numerical simulation, experiment, and optimization of a multidirectional die forging process for oil cutoff valves. Mater Today Commun 33:104838. https://doi.org/10.1016/j.mtcomm.2022.104838
2. Luo S, Yao J, Li J, Du H, Liu H, Yu F (2020) Influence of forging velocity on temperature and phases of forged Ti-6Al-4V turbine blade. J Mater Res Technol 9(6):12043–12051. https://doi.org/10.1016/j.jmrt.2020.08.106
3. Allam Z, Becker E, Baudouin C, Bigot R, Krumpipe P (2014) Forging process control: influence of key parameters variation on product specifications deviations. Procedia Eng 81:2524–2529. https://doi.org/10.1016/j.proeng.2014.10.361
4. Behrens B-A et al (2020) A combined numerical and experimental investigation on deterministic deviations in hot forging processes. Procedia Manuf 47:295–300. https://doi.org/10.1016/j.promfg.2020.04.231
5. Chabeauti H, Ritou M, Lavisse B, Germain G, Charbonnier V (2022) Numerical investigation and modeling of residual stress field variability impacting the machining deformations of forged part. Procedia CIRP 108:687–692. https://doi.org/10.1016/j.procir.2022.04.079
6. Zhang SH, Zhao DW, Gao CR, Wang GD (2012) Analysis of asymmetrical sheet rolling by slab method. Int J Mech Sci 65(1):168–176. https://doi.org/10.1016/j.ijmecsci.2012.09.015
7. Yin J, Hu R, Shu X (2021) Closed-die forging process of copper alloy valve body: finite element simulation and experiments. J Mater Res Technol 10:1339–1347. https://doi.org/10.1016/j.jmrt.2020.12.087
8. Alizadeh R, Allen JK, Mistree F (2020) Managing computational complexity using surrogate models: a critical review. Res Eng Des 31(3):275–298. https://doi.org/10.1007/s00163-020-00336-7
9. Jia L, Alizadeh R, Hao J, Wang G, Allen JK, Mistree F (2020) A rule-based method for automated surrogate model selection. Adv Eng Inform 45:101123. https://doi.org/10.1016/j.aei.2020.101123

10. Scandola L et al (2021) Development of a numerical compensation framework for geometrical deviations in bulk metal forming exploiting a surrogate model and computed compatible stresses. Int J Mater Form 14(5):901–916. https://doi.org/10.1007/s12289-020-01603-7
11. Maier D, Hartmann C, Till M, Büdenbender C, Behrens BA, Volk W (2019) Data-driven compensation for bulk formed parts based on material point tracking. Key Eng Mater 794:277–284. https://doi.org/10.4028/www.scientific.net/KEM.794.277
12. Slimani K, Zaaf M, Balan T (2023) Accurate surrogate models for the flat rolling process. Int J Mater Form 16. https://doi.org/10.1007/s12289-023-01744-5
13. Wang Q et al (2022) Application of the gradient boosting decision tree in the online prediction of rolling force in hot rolling. Int J Adv Manuf Technol 125(1–2):387–397. https://doi.org/10.1007/s00170-022-10716-z
14. Wang Z, Liu Y, Wang T, Gong D, Zhang D (2023) Prediction model of hot strip crown based on industrial data and hybrid the PCA-SDWPSO-ELM approach. Soft Comput 27:1–17. https://doi.org/10.1007/s00500-023-07895-6
15. Song L, Xu D, Wang X, Yang Q, Ji Y (2022) Application of machine learning to predict and diagnose for hot-rolled strip crown. Int J Adv Manuf Technol 120(1–2):881–890. https://doi.org/10.1007/s00170-022-08825-w
16. Wang Z, Huang Y, Liu Y, Wang T (2023) Prediction model of strip crown in hot rolling process based on machine learning and industrial data. Metals 13:900. https://doi.org/10.3390/met13050900
17. Wang L, He S, Zhao Z, Zhang X (2023) Prediction of hot-rolled strip crown based on Boruta and extremely randomized trees algorithms. J Iron Steel Res Int 30. https://doi.org/10.1007/s42243-023-00964-y
18. Di Schino A, Department of Engineering, University of Perugia, 06125 Perugia, Italy (2021) Open die forging process simulation: a simplified industrial approach based on artificial neural network. AIMSMATES 8(5):685–697. https://doi.org/10.3934/matersci.2021041
19. Uribe D, Durand C, Baudouin C, Krumpipe P, Bigot R (2024) Towards the real-time piloting of a forging process: development of a surrogate model for a multiple blow operation. In: Proceedings of the 14th International Conference on the Technology of Plasticity - Current Trends in the Technology of Plasticity, Cham, pp 377–388. https://doi.org/10.1007/978-3-031-41341-4_39
20. Petkar P, Gaitonde V, Karnik S, Kulkarni V, Raju GT, Davim J (2020) Analysis of forming behavior in cold forging of AISI 1010 steel using artificial neural network. Metals - Open Access Metall J 10:1–24. https://doi.org/10.3390/met10111431
21. Petkar P, Gaitonde V, Kulkarni V, Karnik S, Davim J (2023) A comparative study in forming behavior of different grades of steel in cold forging backward extrusion by integrating Artificial Neural Network (ANN) with Differential Evolution (DE) algorithm. Appl Sci 13:1276. https://doi.org/10.3390/app13031276
22. de Gooijer B, Havinga J, Geijselaers H, Van den Boogaard T (2021) Evaluation of POD based surrogate models of fields resulting from nonlinear FEM simulations. Adv Model Simul Eng Sci 8. https://doi.org/10.1186/s40323-021-00210-8
23. Cueto E, Chinesta F, Huerta A (2014) Model order reduction based on proper orthogonal decomposition. In: Chinesta F, Ladevèze P (eds) Separated representations and PGD-based model reduction: fundamentals and applications. Springer, Vienna, pp 1–26. https://doi.org/10.1007/978-3-7091-1794-1_1
24. Chinesta F, Ladeveze P (2014) Separated representations and PGD-based model reduction: fundamentals and applications. https://doi.org/10.1007/978-3-7091-1794-1
25. Havinga J, Mandal PK, van den Boogaard T (2020) Exploiting data in smart factories: real-time state estimation and model improvement in metal forming mass production. Int J Mater Form 13(5):663–673. https://doi.org/10.1007/s12289-019-01495-2
26. Hamdaoui M, Le Quilliec G, Breitkopf P, Villon P (2014) POD surrogates for real-time multi-parametric sheet metal forming problems. Int J Mater Form 7(3):337–358. https://doi.org/10.1007/s12289-013-1132-0
27. Dang VT, Labergere C, Lafon P (2017) POD surrogate models using adaptive sampling space parameters for springback optimization in sheet metal forming. Procedia Eng 207:1588–1593. https://doi.org/10.1016/j.proeng.2017.10.1053
28. Dang V-T, Labergère C, Lafon P (2019) Adaptive metamodel-assisted shape optimization for springback in metal forming processes. Int J Mater Form 12(4):535–552. https://doi.org/10.1007/s12289-018-1433-4
29. Raseli S, Faisal N, Mahat N (2022) Construction of Cubic Bezier Curve. J Comput Res Innov 7:111–120. https://doi.org/10.24191/jcrinn.v7i2.291
30. Baydas S, Karakas B (2019) Defining a curve as a Bezier curve. J Taibah Univ Sci 13:522–528. https://doi.org/10.1080/16583655.2019.1601913
31. Amaishi T, Tsutamori H, Nishiwaki T, Kimoto T (2020) Description of anisotropic properties of sheet metal based on spline curves and hole expansion test simulation of high-strength steel. Int J Solids Struct 202. https://doi.org/10.1016/j.ijsolstr.2020.07.010
32. Ahn YJ, soo Kim Y, Shin Y (2004) Approximation of circular arcs and offset curves by Bézier curves of high degree. J Comput Appl Math 167(2):405–416. https://doi.org/10.1016/j.cam.2003.10.008
33. Oruç H, Phillips GM (2003) q-Bernstein polynomials and Bézier curves. J Comput Appl Math 151(1):1–12. https://doi.org/10.1016/S0377-0427(02)00733-1
34. Fitter HN, Pandey AB, Patel DD, Mistry JM (2014) A review on approaches for handling Bezier Curves in CAD for manufacturing. Procedia Eng 97:1155–1166. https://doi.org/10.1016/j.proeng.2014.12.394
35. Farin G (2014) Curves and surfaces for computer-aided geometric design: a practical guide. Elsevier
36. Liu Y, Yin G (2020) The Delaunay triangulation learner and its ensembles. Comput Stat Data Anal 152:107030. https://doi.org/10.1016/j.csda.2020.107030
37. Lee S, Quagliato L, Park D, Kwon I, Sun J, Kim N (2021) A new approach to preform design in metal forging processes based on the convolution neural network. Appl Sci 11(17):7948. https://doi.org/10.3390/app11177948
38. Mull J-F, Durand C, Baudouin C, Bigot R (2020) A new tailored solution to predict blow efficiency and energy consumption of hammer-forging machines. Int J Adv Manuf Technol 111(7–8):1941–1954. https://doi.org/10.1007/s00170-020-06237-2